

MASSSES AND ACCRETION RATES OF SUPERMASSIVE BLACK HOLES IN ACTIVE GALACTIC NUCLEI FROM THE INTEGRAL SURVEY

© 2024 G. A. Khorunzhev *, S. Yu. Sazonov , R. A. Burenin and A. Yu. Tkachenko

Space Research Institute, Russian Academy of Sciences, Profsoyuznaya ul. 84/32, Moscow, 117997 Russia

Received December 26, 2011

Abstract—The masses of 68 supermassive black holes (SMBHs) in nearby ($z < 0.15$) active galactic nuclei (AGNs) detected by the INTEGRAL observatory in the hard X-ray energy band (17–60 keV) outside the Galactic plane ($|b| > 5^\circ$) have been estimated. Well-known relations between the SMBH mass and (1) the infrared luminosity of the stellar bulge (from 2MASS data) and (2) the characteristics of broad emission lines (from RTT-150 data) have been used. A comparison with the more accurate SMBH mass estimates obtained by the reverberation-mapping technique and from direct dynamical measurements is also made for several objects. The SMBH masses derived from the correlation with the bulge luminosity turn out to be systematically higher than the estimates made by other methods. The ratio of the bolometric luminosity to the critical Eddington luminosity has been found for all AGNs. It ranges from 1 to 100% for the overwhelming majority of objects.

DOI: 10.1134/S1063773712080026

Keywords: active galactic nuclei (AGNs), supermassive black holes (SMBHs).

INTRODUCTION

Measuring the masses of supermassive black holes (SMBHs) in galactic nuclei is an important part of the various studies of both the SMBHs themselves and the interrelationship between the evolution of galaxies and the growth of black holes in their central regions. The most reliable known method of determining the SMBH mass involves measuring the kinematics of stars or gas motions in the gravitational field of a central black hole. Unfortunately, since the angular resolution of telescopes is finite, the applicability of this method is so far restricted to nearby galaxies: the dynamical SMBH mass estimates have been obtained for about 50 galactic nuclei (Gültekin et al. 2009), in the overwhelming majority normal (inactive) ones.

Measuring the SMBH masses in active galactic nuclei (AGNs) — Seyfert galaxies and quasars — is of particular interest, because an active growth of black holes occurs in them. The reverberation-mapping technique, applicable to type-1 AGNs (with broad emission lines in the optical spectrum), is deemed to be fairly reliable. It consists in: (1) measuring the size of the broad-line region from the delay between the line and continuum flux variations, (2) measuring the gas velocity dispersion in this region from the line width, and (3) applying the virial theorem to determine the black hole mass from these

two characteristics. The main problem associated with reverberation mapping is the necessity of performing multiple spectrophotometric observations of AGNs for several weeks or months. Therefore, so far the SMBH masses have been measured by this technique only in several tens of Seyfert galaxies and quasars (Kaspi et al. 2000; Peterson et al. 2004).

Since the methods described above, which may be considered direct ones, are difficult to apply, indirect methods are also actively used to estimate the SMBH masses. For example, in the case of type-1 AGNs, an empirical relation between the SMBH mass and broad-line characteristics (width and luminosity) (see, e.g., Vestergaard & Peterson 2006) has been widely used in recent years. A physical justification for the existence of such a relation was offered by Dibai (1977). In recent years, the SMBH masses in AGNs (of both type 1 and type 2) also came to be often estimated from the correlation with the mass or velocity dispersion of the host stellar spheroid — an elliptical galaxy or the bulge of a spherical galaxy (Ferrarese & Merritt 2000; Tremaine et al. 2002; Marconi & Hunt 2003; Gültekin et al. 2009).

An increasingly active use of indirect methods to determine the SMBH masses in AGNs raises the question of how reliable such estimates are. In particular, is it justifiable to use the correlation between the stellar bulge properties and the central SMBH mass established for normal galaxies in the case of

* e-mail: horge@iki.rssi.ru

active galaxies? Previous studies suggested that the ratio of the black hole mass to the bulge mass in AGNs was systematically lower than that in normal galaxies (Wandel 1999). However, it was shown in a number of succeeding papers that AGNs obeyed the same correlation between the SMBH mass and the velocity dispersion in the bulge ($M_{\text{BH}}-\sigma_*$) as did normal galaxies (Nelson et al. 2004; Onken et al. 2004; Woo et al. 2010; Graham et al. 2011), but, at the same time, significant differences in the correlation between the black hole mass and the bulge luminosity were revealed (Nelson et al. 2004; Bentz et al. 2009). The interpretation of these results is complicated by the fact that the M_{BH} estimates used for comparison with the bulge characteristics were obtained mainly by the reverberation-mapping technique and, consequently, were determined to within the normalization factor f in the virial formula (see Eq.9), which can change from object to object by several times. In addition, at least in the case of one type of AGN, namely narrow-line Seyfert 1 galaxies, the fact that the SMBHs have masses considerably lower than those expected from the correlations with the bulge parameters established for normal galaxies may be considered to have been firmly established (Mathur et al. 2001; Wandel 2002; Grupe & Mathur 2004). As an illustration of the existing uncertainty, it can be noted that the sample of 49 galaxies used by (Gültekin et al. 2009) to construct the correlation between the bulge and SMBH masses contains three Seyfert galaxies with highly accurate (based on maser emission) SMBH mass estimates, and the measured black hole mass in one of them (the Circinus galaxy) turns out to be approximately a factor of 30 lower than that expected from the correlation with the stellar velocity dispersion!

In this paper, we applied various known methods to determine the SMBH mass and the ratio of the current accretion rate to the critical one for a representative sample of nearby Seyfert galaxies drawn from the INTEGRAL hard X-ray all-sky survey. This sample has already been used and is being used for various systematic studies of the local population of AGNs. This work also allows us to reach independent conclusions about the applicability of various methods for estimating the SMBH masses in AGNs.

THE SAMPLE

We used the catalog of AGNs (Krivonos et al. 2007; Sazonov et al. 2007), detected in the hard X-ray energy band (17–60 keV) by the IBIS/ISGRI instrument (Ubertini et al. 2003) onboard the INTEGRAL observatory (Winkler et al. 2003) during the first three and a half years of the mission, from October 2002 to June 2006. Here, we use a complete sample of 68 Seyfert 1 (33 objects) and 2 (35 objects) galaxies

that does not include blazars and objects located near the Galactic plane ($|b| < 5^\circ$). All AGNs represent the local Universe (the redshift of the most distant object is $z = 0.14$). The main advantage of the sample is that it was drawn on the basis of hard X-ray observations and, therefore, essentially does not suffer from ordinary selection effects related to the absorption of emission in AGNs or the difficulty of its detection against the galaxy's bright background. It may be considered to be a representative sample of Seyfert galaxies in the sense that it properly reflects the proportion of type-1 and type-2 AGNs in the local Universe and covers almost the entire luminosity function of Seyfert galaxies. This sample has been used and is being actively used to systematically study such properties of the local population of AGNs as the luminosity function and the photoabsorption column density distribution (Sazonov et al. 2007), the total broadband X-ray spectrum of the population (Sazonov et al. 2008), the ratio of the X-ray and infrared luminosities for AGNs (using data from the Spitzer telescope; Sazonov et al. 2012), and the ratio of the X-ray and narrow-line luminosities (Sazonov et al., in preparation). In the subsequent work, it would be interesting to use this sample to investigate how different AGN emission characteristics depend on the SMBH mass and accretion regime.

Basic information about the objects being studied is presented in Table 1. The morphological types and redshifts of the galaxies were taken mainly from the HyperLeda and NED databases. We took the types of AGNs characterizing their optical properties and radio loudness from our previous papers (Sazonov et al. 2007, 2012), where the references to the original sources of information are given. The photometric distances to the objects were calculated from their redshifts for the following cosmological parameters: $H_0=72 \text{ km s}^{-1} \text{ Mpc}^{-1}$, $\Omega_m=0.3$, and $\Omega_\Lambda=0.7$. For several nearby objects, we used more accurate distances from the Nearby Galaxies Catalogue (Tully et al. 2009; Tully 1988). In particular, we used the distances to the objects to calculate the AGN luminosities in the 17–60 keV energy band from the fluxes measured (with an accuracy better than 20%) by the IBIS/ISGRI instrument (Sazonov et al. 2007).

ESTIMATION OF THE SMBH MASSES FROM EMPIRICAL RELATIONS

We applied both well-known indirect methods for determining the SMBH mass described in the Introduction to our objects.

Table 1. Sample of AGNs from the INTEGRAL survey at $|b| > 5^\circ$

Object	N*	Type of galaxy	Type of AGN	z	D (Mpc)	$\lg L_{17-60 \text{ keV}}$ (erg/s)
MRK348	1	S0a	S2	0.015	63.4	43.56
MCG-01-05-047	2	Sc	S2	0.017	72.8	43.02
NGC788	3	S0a	S2	0.014	57.4	43.28
LED A138501	4		S1	0.049	213.3	44.34
MRK1040	5	Sbc	S1.5	0.017	70.7	43.47
IGRJ02343+3229	6	Sb	S2	0.016	68.5	43.34
NGC1068	7	Sb	S2	0.004	14.4*	43.14
NGC1142	8	Sb ⁽¹⁾	S2	0.029	123.0	43.93
1H0323+342	9	Sb? ⁽²⁾	NLS1	0.061	266.7	44.37
NGC1365	10	Sb	S1.8	0.005	17.9*	42.11
3C111	11	E	S1,BLRG	0.049	210.1	44.62
ESO033-G002	12	S0	S2	0.018	76.7	43.14
IRAS05078+1626	13	S0?	S1.5	0.018	75.8	43.61
ESO005-G004	14	Sb	S2	0.006	22.4*	42.18
MRK3	15	S0	S2	0.013	57.0	43.43
MRK6	16	S0a	S1.5	0.019	79.7	43.45
IGRJ07563-4137	17	S0a?	S2	0.021	89.1	43.08
ESO209-G012	18	Sa?	S1.5	0.041	174.4	43.79
IRAS09149-6206	19		S1	0.057	249.8	44.19
MRK110	20	Sa ⁽¹⁾	NLS1	0.035	151.5	44.21
IGRJ09446-2636	21		S1.5	0.142	658.2	45.31
NGC2992	22	Sa	S2	0.008	30.5*	42.76
MCG-5-23-16	23	S0	S2	0.009	35.7	43.18
NGC3081	24	S0a	S2	0.008	32.5*	42.77
ESO263-G013	25	Sb	S2	0.033	142.7	43.72
NGC3227	26	Sa	S1.5	0.004	20.6*	42.67
NGC3281	27	Sab	S2	0.011	45.1	42.98
IGRJ10386-4947	28		S1.5	0.060	262.1	44.09
IGRJ10404-4625	29	S0	S2	0.024	101.7	43.42
NGC3783	30	Sa	S1	0.010	38.5*	43.34
IGRJ12026-5349	31	S0	S2	0.028	119.5	43.62
NGC4151	32	Sab	S1.5	0.003	20.3*	43.37
MRK50	33	S0a ⁽¹⁾	S1	0.023	99.5	43.19
NGC4388	34	Sb	S2	0.008	16.8*	42.79
NGC4395	35	Sm	S1.8	0.001	4.6*	40.60
NGC4507	36	Sab	S2	0.012	49.7	43.51
NGC4593	37	Sb	S1	0.009	39.5*	43.04
NGC4945	38	Scd	S2	0.002	3.8*	41.54
ESO323-G077	39	S0	S1.2	0.015	63.4	43.13
IGRJ13091+1137	40	Sa	XBONG	0.025	106.9	43.68
IGRJ13149+4422	41	Sa	S2	0.037	157.2	43.81
CENA	42	E	S2,NLRG	0.002	3.6*	41.94
MCG-6-30-15	43	S0	S1.2	0.008	32.4	42.66
MRK268	44	Sb ⁽¹⁾	S2	0.040	171.8	43.79
IC4329A	45	S0a	S1.2	0.016	67.7	43.95
NGC5506	46	Sa	S1.9	0.006	28.7*	43.12
IGRJ14552-5133	47	Sc	NLS1	0.016	67.7	42.89
IGRJ14561-3738	48	Sa	S2	0.025	104.7	43.27
IC4518A	49		S2	0.016	66.4	43.11
WKK6092	50	Sb	S1	0.016	65.9	42.94
IGRJ16185-5928	51	Sc	NLS1	0.035	150.1	43.67
ESO137-G34	52	S0a	S2	0.009	38.7	42.48
IGRJ16482-3036	53		S1	0.031	133.9	43.75
NGC6221	54	Sc	S2	0.005	19.4*	41.94
IGRJ16558-5203	55		S1.2	0.054	234.9	44.29
NGC6300	56	Sb	S2	0.004	14.3*	42.07
IGRJ17418-1212	57		S1	0.037	159.8	43.90
3C390.3	58	E	S1,BLRG	0.056	244.4	44.65
IGRJ18559+1535	59		S1	0.084	372.3	44.58
1H1934-063	60	E	NLS1	0.011	44.6	42.63
NGC6814	61	Sbc	S1.5	0.005	22.8*	42.47
CYGA	62	E	S2,NLRG	0.056	244.4	44.62
IGRJ20286+2544	63	Sd	S2	0.014	60.0	43.16
MRK509	64	S0a ⁽¹⁾	S1.2	0.034	147.5	44.16
NGC7172	65	Sa	S2	0.009	33.9*	42.92
MR2251-178	66	E ⁽³⁾	S1	0.064	280.4	44.65
NGC7469	67	Sa	S1.2	0.016	68.9	43.43
MRK926	68	S0a ⁽¹⁾	S1.5	0.047	203.0	44.25

Note. (1) Petrosian et al. (2007), (2) Zhou et al. (2007), (3) Norgaard-Nielsen et al. (1986). The optical and radio types of AGNs: S1-S2 — Seyfert galaxy, NLS1 — narrow-line Seyfert 1 galaxy, BLRG — broad-line radio galaxy, NLRG — narrow-line radio galaxy, XBONG — X-ray bright optically normal galaxy; z is the redshift; D is the photometric distance ($H_0=72 \text{ km s}^{-1} \text{ Mpc}^{-1}$, $\Omega_m=0.3$, $\Omega_\Lambda=0.7$). For several nearby objects, we used accurate distances (marked by the asterisk) from the Nearby Galaxies Catalogue (Tully et al. 2009; Tully 1988). $L_{17-60 \text{ keV}}$ is the 17–60 keV (INTEGRAL/IBIS/ISGRI) AGN luminosity.

*ESTIMATION FROM THE INFRARED BULGE
LUMINOSITY (BASED ON 2MASS DATA)*

In the last 10–15 years, the existence of a correlation between the SMBH mass and properties of the spheroidal component of the host galaxy, i.e., the bulge of a spiral galaxy or an entire elliptical galaxy, has been firmly established. At the same time, the question of precisely which characteristic of the spheroid (mass, luminosity, velocity dispersion, etc.) correlates more closely with the central black hole mass remains open, because different constructed correlations are characterized by approximately the same dispersion—the scatter of individual values about the mean (see, Marconi & Hunt 2003; Graham 2007; Gültekin et al. 2009). As has already been said, any such correlations were firmly established only for normal (inactive) galaxies, while their applicability for AGNs is still open to question.

In this paper, we used the correlation between the SMBH mass and the near-infrared luminosity of the bulge/elliptical galaxy (Graham 2007):

$$\lg M_{\text{BH}} = -0.37(\pm 0.04)(M_{K,b} + 24) + 8.29(\pm 0.08), \quad (1)$$

where M_{BH} is the black hole mass in solar masses, and $M_{K,b}$ is the extinction-corrected K -band absolute magnitude of the bulge (or elliptical galaxy).

The empirical relation (1) was constructed by Graham from 21 nearby galaxies with available dynamical SMBH mass measurements. The scatter of $\lg M_{\text{BH}}$ in this sample about the mean (including the measurement errors) is 0.33.

For our purposes, it is convenient to rewrite relation (1) via the bulge luminosity $L_{K,b}$ (using the characteristics of the 2MASS K_S filter: the central wavelength is $2.16 \mu\text{m}$, the bandwidth is 1.686×10^{13} Hz, and the spectral flux density corresponding to the zero magnitude is 666.7 Jy):

$$\lg M_{\text{BH}} = 0.925 \lg L_{K,b} - 31.23, \quad (2)$$

where $L_{K,b}$ is measured in erg/s.

The $M_{\text{BH}}-L_{K,b}$ correlation is essentially equivalent to the SMBH mass–bulge mass correlation, because the infrared luminosity of galaxies is roughly proportional to their stellar mass. We preferred to use precisely this relation, mainly because almost for all our objects the infrared luminosity of a galaxy can be easily estimated from the publicly accessible data of the Two-Micron All-Sky Survey (2MASS), which covered 99% of the sky in three bands: $J(\lambda = 1.24 \mu\text{m})$, $H(\lambda = 1.66 \mu\text{m})$ and $K_S(\lambda = 2.16 \mu\text{m})$.

Most (62) objects of our sample are present either in the Extended Source Catalog (XSC, Jarrett et al. 2000) or in the Large Galaxy Atlas (LGA, Jarrett et al. 2003) of 2MASS, where the apparent K magnitude

(m_K) of the entire galaxy is given. This allowed us to determine the total infrared luminosities of the galaxies (L_K) corrected for interstellar extinction (Table 2).

The active nucleus can contribute noticeably to the galaxy’s infrared luminosity, because part of the emission (mainly the ultraviolet one) from the SMBH accretion disk is absorbed and reprocessed in the surrounding torus of gas and dust. We attempted to estimate this contribution,

$$P_{\text{AGN}} = \frac{L_{K,\text{AGN}}}{L_K}, \quad (3)$$

using the correlation between the infrared and hard X-ray AGN luminosities. Such a correlation was firmly established, for example, in our recent paper (Sazonov et al. 2012) through observations of the same AGN sample from the INTEGRAL survey that is used here with the Spitzer infrared telescope. It follows from the results of this paper and a number of published spectral energy distributions averaged over representative samples of quasars (Elvis et al. 1994; Sazonov et al. 2004; Richards et al. 2006; Shang et al. 2011) that the K -band luminosity of the dusty torus is

$$L_{K,\text{AGN}} \sim 0.1 L_{17-60 \text{ keV}}, \quad (4)$$

where $L_{17-60 \text{ keV}}$ is the AGN luminosity measured in the INTEGRAL energy band (Table 1). In this case, the ratio $L_{K,\text{AGN}}/L_{17-60 \text{ keV}}$ can vary from object to object by a factor of ~ 2 .

The values of P_{AGN} found from Eqs. (3) and (4) are given in Table 2. For the Seyfert galaxy NGC 1068, the dusty torus is optically thick for Compton scattering. Therefore, the luminosity measured by INTEGRAL accounts for only a small fraction (of the order of one percent; see, e.g., Sazonov et al. 2012) of the true hard X-ray luminosity of the hot accretion disk corona. We estimated this luminosity from Eqs. (15) and (16) given below and only then did we calculate P_{AGN} from Eqs. (3) and (4).

The effective angular size of the galaxy in the 2MASS image (R_{eff}), the radius within which half of the galaxy’s total K -band luminosity is contained, can serve as an additional indicator of the contribution from the active nucleus to the galaxy’s infrared luminosity. The values of R_{eff} from the XSC and LGA are listed in Table 2. They should be compared with the 2MASS angular resolution, which is $\sim 2''.5$ (Skrutskie et al. 2006): if R_{eff} is only a few arcsec, then this may indicate that the contribution from the active nucleus to L_K is dominant. However, in this case, it should be kept in mind that the angular size of the galaxy can be small per se for the most distant objects of our sample.

For 17 objects, the contribution from the active nucleus to the galaxy’s infrared luminosity estimated

from the X-ray luminosity turned out to be greater than 50% ($P_{\text{AGN}} > 0.5$). Therefore, (given some uncertainty associated with Eq. (4)) it turns out to be impossible to reliably subtract the AGN contribution from the galaxy's total luminosity for such objects, and the values of L_K measured for them can be used only to obtain upper limits on the SMBH mass from its correlation with the bulge luminosity. In addition, in all these cases, except for MRK 348 and CYG A, the galaxy's size $R_{\text{eff}} \lesssim 5''$, which also indirectly points to a substantial contribution from the central dusty torus to L_K .

The next step in our calculations is to estimate the bulge fraction (P_b) in the galaxy's K-band luminosity (i.e., basically the bulge mass fraction). Unfortunately, an accurate allowance cannot be made for most of the sample objects, because many of the galaxies are at a distance of the order of or greater than 100 Mpc and there are no optical or infrared (2MASS) images for them with an angular resolution high enough for the nucleus, bulge, and disk emission components to be reliably separated. Therefore, we decided to resort to a less accurate method, more specifically, to assign some mean expected values of P_b to the galaxies based on their morphological types listed in Table 1. This approach is justified, because the bulge mass fraction correlates with the type of galaxy, although there exists an appreciable scatter of P_b values among galaxies of the same type. There is no uncertainty only for elliptical galaxies, for which, obviously, $P_b = 1$. For the remaining types, we adopted the following values based on the results from Laurikainen et al. 2007; Graham & Worley 2008; Laurikainen et al. 2010: $P_b = 0.25$ (S0–Sab), 0.2 (Sb), 0.13 (Sbc), 0.08 (Sc), 0.06 (Scd and later types). For four galaxies (IGR J09446-2636, IGR J10386-4947, IGR J16482-3036, IGR J18559+1535) whose morphological types were not established but which, nevertheless, are present in the 2MASS XSC, we adopted $P_b = 0.25$ as a rough estimate of the bulge fraction.

Thus, we calculated the K-band bulge luminosity for most of the objects as

$$L_{K,b} = P_b(1 - P_{\text{AGN}})L_K, \quad (5)$$

and obtained the following upper limits for the objects in which the AGN contribution is dominant ($P_{\text{AGN}} > 0.5$):

$$L_{K,b} < P_b L_K. \quad (6)$$

Five objects (IRAS 05078+1626, IRAS 09149-6206, IC 4518A, IGR J16558-5203, IGR J17418-1212) enter neither into the Extended Source Catalog nor into the Large Galaxy Atlas, but they are contained only in the 2MASS Point Source Catalog (PSC, Skrutskie et al. 2006). Since the method of calculation described above

cannot be used for these objects, we made rougher estimates of the bulge luminosity for them as follows. The PSC provides the apparent K magnitudes of the sources measured in an aperture with a radius of $4''$. This angular size corresponds to a linear size from ~ 1.3 to ~ 5 kpc for the galaxies listed above, i.e., it roughly corresponds to the size of the bulges in typical galaxies. Therefore, we assumed that the measured magnitude of the point infrared source roughly corresponded to the luminosity of the galactic bulge, from which, however, the expected AGN fraction should be subtracted. Thus, we used modified formulas for these five objects:

$$P_{\text{AGN}} = \frac{L_{K,\text{AGN}}}{L_{K,\text{PSC}}}, \quad (7)$$

$$L_{K,b} = (1 - P_{\text{AGN}})L_{K,\text{PSC}}, \quad (8)$$

where $L_{K,\text{PSC}}$ is the luminosity of the PSC point source.

Since the Seyfert galaxy LEDA 138501 is close to the Galactic plane in the sky, there are no reliable 2MASS photometric data for it. In addition, the morphological type of the galaxy is unknown. As a result, this is the only object for which even a reliable upper limit on the SMBH mass cannot be established from its correlation with the stellar bulge luminosity. The SMBH mass estimates (or upper limits) for the remaining 67 objects are presented in Table 2.

Apart from the M_{BH} estimates themselves, their uncertainties are also important. Since all of the objects being studied are bright 2MASS sources, the errors related to the photometric measurements of their infrared luminosities may be neglected. The main uncertainty in our calculations is associated with the determination of the bulge fraction in the galaxy's infrared luminosity. Based on the results of the statistical studies of galaxies mentioned above (see, e.g., Laurikainen et al. 2010), we can estimate the systematic error in $\lg P_b$ and, consequently, $\lg L_{K,b}$ from Eq. (5) for galaxies with known morphological types to be ~ 0.3 , i.e., the bulge luminosity can be determined to within a factor of 2. For galaxies with unknown morphologies, the error in $\lg L_{K,b}$ is, obviously, ~ 0.5 —this corresponds to a scatter of P_b values from ~ 0.08 to ~ 0.8 about the presumed value of 0.25, i.e., almost any type of galaxy is admitted. The same large error (~ 0.5) can also be assigned to the objects for which the bulge luminosity was estimated from the luminosity of the PSC point infrared source. Finally, we can assign an uncertainty of ~ 0.1 to the values of $\lg L_{K,b}$ obtained for elliptical galaxies to take into account the photometric measurement errors in 2MASS. Because of the approximate proportionality of relation (2) between $L_{K,b}$ and M_{BH} , the ultimate errors in $\lg M_{\text{BH}}$ found from the correlation with the bulge luminosity are expected to be the same as the errors in

$\lg L_{K,b}$ given above. These uncertainties are taken into account in the subsequent statistical analysis.

Of course, the considerable uncertainty can also be associated with the very use of the $M_{BH}-L_{K,b}$ correlation to determine the SMBH masses in the AGNs of our sample, but we can attempt to estimate its value only by comparing the mass estimates obtained by this method with those obtained by other methods (see below).

*ESTIMATION FROM BROAD-LINE
PARAMETERS (BASED ON RTT-150
OBSERVATIONS)*

The broad emission lines present in the spectra of type-1 AGNs originate in the clouds of photoionized gas located inside the sphere of gravitational influence of the SMBH. This provides the fundamental possibility of using the virial theorem to determine the SMBH mass:

$$M_{BH} = f \frac{Rv^2}{G}, \quad (9)$$

where R is the characteristic distance from the SMBH at which the emission in a particular broad line is generated, v is the gas velocity dispersion in this region, G is the gravitational constant, and f is a coefficient dependent on the structure and orientation of the broad-line region.

The characteristic velocity v is easy to estimate from the Doppler broadening of spectral lines. As regards the size of the region R , it can be measured by the reverberation-mapping technique. However, this suggests a spectroscopic monitoring of AGNs for many nights, which is by no means always possible. Therefore, in recent years, an indirect method based on the estimation of the size of the broadline region from the AGN luminosity (L) either in the broadest line or in the continuum has been actively used. Dibai (1977) predicted a power law $R \propto L^\alpha$ with a slope $\alpha = 1/3$. It follows from reverberation measurements that $\alpha \sim 0.5-0.7$ (Wandel et al. 1999; Kaspi et al. 2000, 2005; Vestergaard & Peterson 2006). The fundamental advantage of this method is that the SMBH mass in AGNs can be estimated from a single measurement of the line width and the line or continuum luminosity.

We applied the empirical relation between M_{BH} and parameters of the broad Balmer H_β line ($\lambda = 4861 \text{ \AA}$) from (Vestergaard & Peterson 2006) to estimate the SMBH masses in the type-1 AGNs from our sample:

$$\lg M_{BH} = \lg \left[\left(\frac{FWHM(H_\beta)}{1000 \text{ km s}^{-1}} \right)^2 \times \left(\frac{L(H_\beta)}{10^{42} \text{ erg s}^{-1}} \right)^{0.63} \right] + 6.67, \quad (10)$$

where the black hole mass M_{BH} is in solar masses, $FWHM$ is the full width at half maximum of the line, and L is the line luminosity corrected for the absorption on the line of sight. Relation (10) is characterized by an intrinsic scatter (of $\lg M_{BH}$ values about the mean) of ~ 0.43 (Vestergaard & Peterson 2006).

It is important to note that the virial formula (9) is defined to within the scale factor f , because there exists a fundamental uncertainty in how the gas velocity field is structured in the broad-line regions. For example, $f = 3$ for a spherically symmetric broad-line region (Wandel et al. 1999; Kaspi et al. 2000) and $f \rightarrow \infty$ for a Keplerian disk whose plane is oriented toward the observer. Therefore, in several papers, the mean $\langle f \rangle$ for the sample was found in such a way that the SMBH masses measured by the reverberation technique satisfied the $M_{BH}-\sigma_*$ correlation for normal galaxies. Onken et al. (2004) obtained $\langle f \rangle = 5.5$ precisely in this way. This value was then used by Vestergaard & Peterson 2006 to derive the empirical formula (10). Thus, this formula implies that the standard $M_{BH}-\sigma_*$ relation must hold for AGNs.

In 2008–2010, a series of spectroscopic observations was performed with the Russian-Turkish 1.5-m telescope (RTT-150) for a sample of 19 Seyfert 1 galaxies from the INTEGRAL survey with declinations $\delta > -20^\circ$. The observations were carried out with the TFOSC low- and medium-resolution spectrometer. At the first stage of these observations, broadband (3230–9120 Å) spectra were taken for all objects with a resolution of 12 Å using grism #15 and a 67- μm (1.74-arcsec) slit. Subsequently, higher resolution spectra were taken for some of the objects in the 3900–6800 Å band with a resolution of 4 Å (grism #7, a 54 μm slit, 1.40 arcsec) and the 5850–8270 Å band with a resolution of 3 Å (grism #8, a 54- μm slit, 1.40 arcsec).

We reduced the optical observations and calibrated the spectra using the *IRAF*¹ standard software. The bias image was subtracted from the two-dimensional spectra; subsequently, the images were aligned using the flat-field spectra obtained from the spectrum of a halogen lamp. The one-dimensional spectra of the objects were extracted in a linear aperture that was centered on the object's emission maximum and had a size large enough for only a negligible fraction of the flux in broad Balmer lines to fall outside this aperture. The spectral density of the emission was calibrated in a standard way using observations of spectrophotometric standard stars.

In most cases, because of the atmospheric jitter, the angular resolution during our observations was such that the size of a point source exceeded the slit size. Therefore, we corrected the fluxes in all of our spectra for the slit by assuming the slit to cut off part of the

¹<http://iraf.noao.edu>

Table 2. Estimates of the SMBH masses from their correlation with the bulge luminosity

Object	N ^a	R_{eff} (arcsec)	m_K	A_K	$\lg L_K$ (erg/s)	P_{AGN}	P_b	$\lg L_{K,b}$ (erg/s)	$\lg M_{\text{BH}}$ (M_\odot)
MRK348	1	9.0	10.10	0.024	42.70	0.72	0.25	< 42.10	< 7.71
MCG-01-05-047	2	23.9	9.39	0.010	43.10	0.08	0.08	41.97	7.58
NGC788	3	14.0	9.07	0.010	43.02	0.18	0.25	42.33	7.92
LEDA138501	4								
MRK1040	5	17.8	9.27	0.035	43.13	0.22	0.13	42.14	7.75
IGRJ02343+3229	6	24.1	8.77	0.036	43.31	0.11	0.2	42.56	8.13
NGC1068	7	15.2	5.79	0.012	43.13	0.30	0.2	42.28	7.88
NGC1142	8	27.0	9.02	0.026	43.71	0.16	0.2	42.94	8.48
1H0323+342	9	2.4	11.79	0.078	43.30	1.19	0.2	< 42.60	< 8.17
NGC1365	10	59.5	6.37	0.007	43.09	0.01	0.2	42.38	7.97
3C111	11	3.1	11.38	0.605	43.46	1.44	1	< 43.46	< 8.97
ESO033-G002	12	6.0	10.03	0.053	42.91	0.17	0.25	42.23	7.82
IRAS05078+1626	13		*11.61	0.110	42.29	2.10		\gtrsim 42.29	\gtrsim 7.88
ESO005-G004	14	27.5	8.14	0.052	42.59	0.04	0.2	41.88	7.50
MRK3	15	8.6	8.97	0.069	43.08	0.22	0.25	42.37	7.96
MRK6	16	2.8	9.56	0.050	43.13	0.21	0.25	42.42	8.01
IGRJ07563-4137	17	5.2	10.13	0.283	43.09	0.10	0.25	42.44	8.02
ESO209-G012	18	4.2	10.09	0.095	43.62	0.15	0.25	42.94	8.49
IRAS09149-6206	19		*9.43	0.067	44.18	0.10		\leq 44.13	\leq 9.59
MRK110	20	2.2	11.80	0.005	42.77	2.74	0.25	< 42.17	< 7.77
IGRJ09446-2636	21	2.5	12.71	0.031	43.69	4.14	*0.25	\gtrsim 43.09	\gtrsim 8.62
NGC2992	22	14.2	8.60	0.022	42.67	0.12	0.25	42.01	7.62
MCG-5-23-16	23	5.2	9.35	0.040	42.51	0.47	0.25	41.63	7.28
NGC3081	24	21.6	8.91	0.020	42.60	0.15	0.25	41.92	7.55
ESO263-G013	25	17.9	10.53	0.062	43.25	0.30	0.2	42.40	7.98
NGC3227	26	38.7	7.64	0.008	42.70	0.09	0.25	42.06	7.67
NGC3281	27	32.6	8.31	0.035	43.13	0.07	0.25	42.49	8.07
IGRJ10386-4947	28	2.2	11.82	0.179	43.31	0.60	*0.25	\gtrsim 42.71	\gtrsim 8.27
IGRJ10404-4625	29	5.4	10.38	0.058	43.01	0.25	0.25	42.28	7.88
NGC3783	30	11.9	8.65	0.044	42.86	0.30	0.25	42.10	7.71
IGRJ12026-5349	31	2.6	9.95	0.075	43.33	0.19	0.25	42.64	8.20
NGC4151	32	16.6	7.38	0.010	42.80	0.38	0.25	41.99	7.61
MRK50	33	3.5	12.00	0.006	42.33	0.73	0.25	< 41.73	< 7.36
NGC4388	34	36.1	8.00	0.012	42.38	0.26	0.2	41.56	7.20
NGC4395	35	48.5	9.98	0.006	40.47	0.14	0.06	39.18	5.01
NGC4507	36	11.9	8.87	0.036	42.99	0.33	0.25	42.21	7.81
NGC4593	37	30.2	7.99	0.009	43.13	0.08	0.2	42.40	7.98
NGC4945	38	172.7	4.48	0.065	42.52	0.01	0.06	41.30	6.96
ESO323-G077	39	3.0	8.80	0.037	43.23	0.08	0.25	42.59	8.16
IGRJ13091+1137	40	9.9	10.18	0.009	43.12	0.36	0.25	42.32	7.91
IGRJ13149+4422	41	6.0	10.82	0.007	43.20	0.41	0.25	42.36	7.95
CENA	42	82.6	3.94	0.042	42.68	0.02	1	42.67	8.24
MCG-6-30-15	43	3.2	9.58	0.023	42.33	0.22	0.25	41.62	7.26
MRK268	44	4.5	10.88	0.006	43.25	0.35	0.2	42.37	7.95
IC4329A	45	2.7	8.80	0.022	43.28	0.47	0.25	42.40	7.98
NGC5506	46	12.4	8.19	0.022	42.78	0.22	0.25	42.07	7.68
IGRJ14552-5133	47	6.7	10.36	0.243	42.74	0.14	0.08	41.58	7.23
IGRJ14561-3738	48	9.6	9.63	0.031	43.33	0.09	0.25	42.69	8.25
IC4518A	49		*11.73	0.058	42.10	1.01		\gtrsim 42.10	\gtrsim 7.71
WKK6092	50	12.1	10.24	0.071	42.70	0.17	0.2	41.92	7.54
IGRJ16185-5928	51	4.0	11.14	0.118	43.07	0.40	0.08	41.76	7.39
ESO137-G34	52	23.7	8.26	0.123	43.05	0.03	0.25	42.44	8.02
IGRJ16482-3036	53	3.0	11.34	0.124	42.90	0.71	*0.25	\gtrsim 42.30	\gtrsim 7.89
NGC6221	54	42.4	7.12	0.061	42.88	0.01	0.08	41.78	7.41
IGRJ16558-5203	55		*10.88	0.142	43.58	0.52		\gtrsim 43.58	\gtrsim 9.07
NGC6300	56	54.3	6.93	0.036	42.68	0.02	0.2	41.97	7.59
IGRJ17418-1212	57		*11.29	0.210	43.10	0.62		\gtrsim 43.10	\gtrsim 8.64
3C390.3	58	2.1	11.54	0.026	43.30	2.24	1	\gtrsim 43.30	\gtrsim 8.82
IGRJ18559+1535	59	4.3	12.53	0.346	43.40	1.53	*0.25	\gtrsim 42.79	\gtrsim 8.35
1H1934-063	60	5.3	9.67	0.108	42.60	0.11	1	42.56	8.13
NGC6814	61	31.8	7.66	0.067	42.81	0.05	0.13	41.90	7.53
CYGA	62	13.4	10.28	0.140	43.85	0.59	1	< 43.85	< 9.33
IGRJ20286+2544	63	8.1	9.87	0.164	42.80	0.23	0.06	41.47	7.12
MRK509	64	2.1	10.01	0.021	43.47	0.49	0.25	42.58	8.15
NGC7172	65	19.0	8.32	0.010	42.87	0.11	0.25	42.21	7.81
MR2251-178	66	1.9	11.13	0.014	43.58	1.18	1	< 43.58	< 9.08
NGC7469	67	4.7	8.85	0.025	43.28	0.14	0.25	42.61	8.18
MRK926	68	5.4	10.64	0.015	43.49	0.57	0.25	< 42.89	< 8.44

Note. R_{eff} is the effective angular size of the galaxy (from the XSC and LGA of 2MASS); m_K is the apparent magnitude of the entire galaxy (from the XSC and LGA), or (marked by the asterisk) the point source (from the PSC of 2MASS); A_K is the interstellar extinction toward the source (Schlegel et al. 1998); L_K is the extinction-corrected luminosity of the entire galaxy or the PSC point source; P_{AGN} is the AGN fraction in L_K ; P_b is the bulge mass fraction taken to be 0.25 in the absence of morphological information about the galaxy (marked by the asterisk); $L_{K,b}$ is the bulge luminosity; M_{BH} is the SMBH mass.

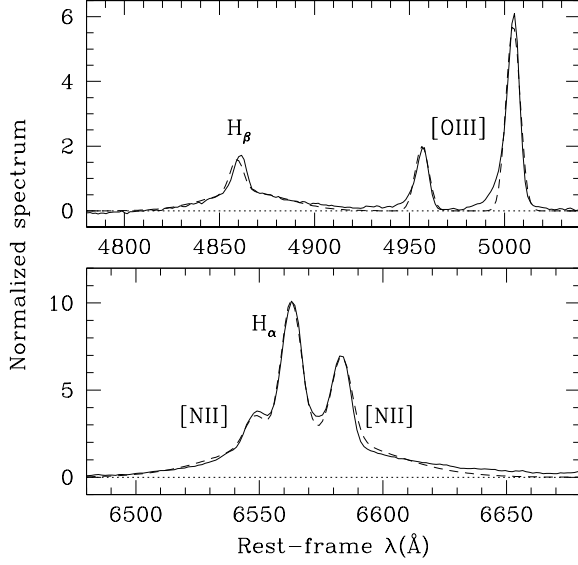


Fig. 1. Example of modeling the RTT-150 spectrum. The solid curve indicates the spectrum of the Seyfert galaxy NGC 7469 near H_β and H_α taken with a resolution ~ 4 Å. The model (dashed curve) includes the broad and narrow Balmer lines as well as the narrow forbidden [OIII] and [NII]. The continuum was described by a polynomial and was subtracted.

flux from a source in the shape of a two-dimensional Gaussian.

The subsequent scientific analysis consisted in subtracting the continuum described by a high-degree polynomial and modeling the line spectra near H_α и H_β . The model of the spectrum near H_β consisted of broad and narrow allowed H_β lines ($\lambda = 4861.3$ Å) and two forbidden [OIII] lines ($\lambda_1 = 4958.9$, $\lambda_2 = 5006.8$ Å). The ratio of the [OIII] doublet line fluxes was fixed: $F_2/F_1 = 2.91$. The profiles of all lines were assumed to be Gaussian. The intensity, broadening (measured in km/s), and systemic velocity of all the listed lines were free model parameters, but the broadenings and velocities of all narrow (H_β и [OIII]) lines were assumed to be identical (which is reasonable, because these lines originate approximately in the same gas). For the spectrum near H_α , we used a similar model that, in addition to the broad and narrow H_α lines, included the doublet of forbidden [NII] lines ($\lambda_1 = 6548.0$, $\lambda_2 = 6583.4$ Å, $F_2/F_1 = 2.96$). The broadenings and velocities of the narrow H_α and [NII] lines were assumed to be identical. All of the measured line broadenings were then corrected for the spectral resolution of the measurements.

The described model allowed the parameters of the lines of interest to us to be measured fairly reliably

for most of the objects (Table 3). For the narrow-line Seyfert 1 galaxy 1H 0323+342, we used a simplified model in which the H_α and H_β lines had only broad components (nevertheless, the complete model was used for two other AGNs of the same type, MRK 110 and 1H 1934-063), because the narrow components of the Balmer lines could not be distinguished. An example of modeling the spectrum is shown in Fig. 1. The broad lines in the spectra of two objects, MRK 6 and 3C 390.3, have a complex shape and are poorly described by a Gaussian. Therefore, the parameters measured for them cannot be considered reliable and were excluded from the subsequent analysis.

The extinction in the path from the broad-line region to the observer was estimated from the ratio of the Balmer-line fluxes (Balmer decrement):

$$A_{V,\text{Balm}} = 7.21 \lg \frac{F(H_\alpha)}{B_0 F(H_\beta)}, \quad (11)$$

where $B_0 = F_0(H_\alpha)/F_0(H_\beta)$ is the expected Balmer decrement for broad lines in AGNs without extinction, which was assumed to be 3.06 (Dong et al. 2008).

The value of $A_{V,\text{Balm}}$ measured in this way was then compared with the interstellar extinction in our Galaxy toward the object $A_{V,\text{gal}}$ (Schlegel et al. 1998). If $A_{V,\text{Balm}}$ turned out to exceed $A_{V,\text{gal}}$ by more than 1σ (the error of our measurement), then we used $A_V = A_{V,\text{Balm}}$ for the subsequent calculations, i.e., we assumed the broad-line emission to be absorbed not only in the interstellar medium of our Galaxy but also in the object itself (in the galaxy or its nucleus). Otherwise, we used $A_V = A_{V,\text{gal}}$. The final correction of the measured line fluxes for extinction was made by a standard method (Cardelli et al. 1989): $A(H_\alpha) = 0.8177A_V$, $A(H_\beta) = 1.1643A_V$. The derived line luminosities are given in Table 3.

The last column in Table 3 gives the SMBH masses calculated from Eq. (10). The presented errors take into account the uncertainties related to both the measurement of the H_β parameters and the extinction correction. The latter dominates in the objects in which an additional (with respect to the extinction in the Galaxy) extinction was revealed by the Balmer decrement. The uncertainty associated with Eq. (10) itself was disregarded.

COMPARISON OF VARIOUS MASS DETERMINATION METHODS

Table 5 gathers together the various estimates of the SMBH masses in 68 AGNs from the INTEGRAL survey. For 67 objects, we present the estimates (M_{bulge}) based on the infrared luminosity of the bulge/elliptical galaxy obtained from 2MASS data here. For 17 Seyfert 1 galaxies, we present

Table 3. Estimates of the SMBH masses from Balmer-line parameters

Объект	N	$F(H_\alpha)$ (10^{-13} erg s $^{-1}$ cm $^{-2}$)	$F(H_\beta)$ (10^{-13} erg s $^{-1}$ cm $^{-2}$)	$A_{V,Balm}$	$A_{V,gal}$	FWHM(H_α) (km/s)	$\lg L(H_\alpha)$ (erg/s)	FWHM(H_β) (km/s)	$\lg L(H_\beta)$ (erg/s)	$\lg M_{BH}$ (M_\odot)
LED138501	4	8.22±0.20	3.14±0.30	0	0.53	5275±144	42.82±0.01	5981±530	42.48±0.04	8.53±0.08
MRK1040	5	6.13±0.17	1.07±0.11	1.96±0.34	0.32	3125±80	42.21±0.11	4349±497	41.72±0.17	7.77±0.14
1H0323+342	9	1.18±0.17	0.52±0.05	0	0.71	1879±99	42.23±0.06	1634±181	41.98±0.04	7.08±0.10
3C111	11	1.73±0.03	0.12±0.01	4.85±0.32	5.46	4757±89	43.75±0.01	6021±608	43.34±0.04	9.08±0.09
IRAS05078+1626	13	3.33±0.10	0.61±0.08	1.81±0.41	0.99	4034±132	41.95±0.13	4549±608	41.47±0.20	7.65±0.17
MRK110	20	7.38±0.59	2.21±0.10	0.27±0.29	0.04	2546±99	42.32±0.10	2369±141	41.80±0.14	7.29±0.10
NGC3227	26	24.10±1.55	6.52±0.86	0.59±0.46	0.08	3504±200	41.28±0.15	3704±584	40.80±0.22	7.05±0.20
NGC4151	32	75.80±1.98	20.90±1.50	0.53±0.24	0.09	5030±160	41.75±0.08	5430±469	41.26±0.12	7.67±0.10
MRK50	33	2.47±0.11	0.86±0.09	0	0.05	4064±212	41.48±0.02	4192±495	41.03±0.05	7.30±0.11
NGC4593	37	6.74±0.33	2.34±0.26	0	0.08	3645±200	41.13±0.02	4260±563	40.68±0.05	7.10±0.12
IGRJ17418-1212	57	1.19±0.10	0.20±0.07	2.04±1.07	1.90	6137±469	42.18±0.35	5586±1733	41.68±0.52	7.96±0.42
1H1934-063	60	3.80±0.33	1.00±0.14	0.68±0.51	0.97	1768±64	41.27±0.04	1418±200	40.83±0.06	6.24±0.13
NGC6814	61	6.12±0.31	2.04±0.25	0	0.79	2998±146	40.84±0.02	4015±589	40.47±0.05	6.91±0.13
MRK509	64	24.00±0.81	7.23±0.47	0.26±0.23	0.19	4024±127	42.86±0.08	4580±372	42.36±0.11	8.22±0.10
MR2251-178	66	10.80±0.42	3.75±0.49	0	0.13	5564±243	43.05±0.02	6735±791	42.61±0.06	8.71±0.11
NGC7469	67	22.20±0.83	5.89±0.54	0.65±0.31	0.23	3205±118	42.31±0.10	3148±346	41.83±0.15	7.56±0.13
MRK926	68	8.07±0.23	3.00±0.28	0	0.14	6709±250	42.65±0.01	9012±1050	42.24±0.04	8.73±0.10

Note. $F(H_\alpha, H_\beta)$ are the extinction-uncorrected line fluxes; $A_{V,Balm}$ is the extinction from the Balmer-line ratio; $A_{V,gal}$ is the extinction in the Galaxy (Schlegel et al. 1998). FWHM (H_α, H_β) are the full widths at half maximum of the lines; $L(H_\alpha, H_\beta)$ are the extinction-corrected line luminosities (we used the boldfaced value of $A_{V,gal}$ или $A_{V,Balm}$); M_{BH} is the SMBH mass.

Table 4. Cross-correlation of the SMBH masses found by different methods

Correlation	N	$\beta \pm \Delta\beta$	$\alpha \pm \Delta\alpha$	$\epsilon_0 \pm \Delta\epsilon_0$	ρ	P_ρ	r	P_r
$M_{H\beta} - M_{bulge}$	8	-0.12±0.13	-0.16±0.16	~ 0	0.26	0.53	0.06	0.89
$M_{rev} - M_{bulge}$	7	1.20±0.31	0.52±0.35	0.51±0.06	0.29	0.54	0.87	0.01
$M_{rev} - M_{bulge}$ (without NGC 4395)	6	0.11±0.30	-0.05±0.23	~ 0	-0.14	0.79	0.18	0.73
$M_{dyn} - M_{bulge}$	4	0.46±0.32	0.01±0.35	~ 0	0.20	0.80	0.72	0.28
$M_{rev} - M_{H\beta}$	6	0.73±0.42	-0.05±0.30	0.34±0.05	0.26	0.62	0.60	0.21

Note. N is the number of objects; ρ is the Spearman rank correlation coefficient; P_ρ is the probability that the null hypothesis holds; r is the Pearson correlation coefficient; P_r is the probability that the null hypothesis holds.

the estimates ($M_{H\beta}$) based on the parameters of the broad H_β line that we obtained from RTT-150 data. In addition, for ten Seyfert 1 galaxies, we provide the reverberation-based measurements (M_{rev}) (Peterson et al. 2004; Onken & Peterson 2002; Peterson et al. 2005; Denney et al. 2006). Finally, for five objects, we give the masses (M_{dyn}) measured from the kinematics of the stars or gas near the SMBH (Gültekin et al. 2009).

The various estimates of the SMBH masses in the AGNs of our sample are compared in Figs. 2 and 3. To get a quantitative idea of how the various methods agree between themselves, we calculated the linear regression:

$$y = \alpha + \beta x, \quad x = \lg \frac{M_1}{10^8 M_\odot}, \quad y = \lg \frac{M_2}{10^8 M_\odot}, \quad (12)$$

where M_1 and M_2 are the SMBH masses estimated by two different methods. Normalizing the masses to $10^8 M_\odot$ (a typical value for our sample) allows the correlation between the regression parameters α and β to be minimized.

In our calculations, we used the technique described in Tremaine et al. 2002 and the FITEXY algorithm (Press et al. 1992). More specifically, the regression parameters α and β are found by minimizing the

function χ^2 :

$$\chi^2 = \sum_{i=1}^N \frac{(y_i - \alpha - \beta x_i)^2}{\epsilon_{yi}^2 + \epsilon_0^2 + \beta^2 \epsilon_{xi}^2}, \quad (13)$$

where x_i and y_i are the estimates for the i th object, ϵ_{xi} and ϵ_{yi} are the corresponding errors, and ϵ_0 is the intrinsic scatter of the correlation. The value of ϵ_0 is determined when χ^2 divided by the number of degrees of freedom becomes equal to one. The errors of α , β , and ϵ_0 are found by varying the parameters within the range defined by the condition $\chi^2 - \chi_{min}^2 \leq 1$.

Table 4 presents the results of our cross-correlation analysis of the SMBH mass estimate from the bulge luminosity (M_{bulge}), which was used as the variable y in Eq. (12), with other types of estimates ($M_{H\beta}$, M_{rev} , M_{dyn}). The result of a similar comparison of M_{rev} with $M_{H\beta}$ is also presented. In our calculations, we disregarded the upper limits on the mass available for several objects.

We found no statistically significant correlation between M_{rev} and $M_{H\beta}$. This is not surprising, because only six objects were compared. However, this comparison confirms the validity of the empirical formula (10) for Seyfert galaxies, because no systematic bias of the $M_{H\beta}$ estimates relative to the M_{rev} estimates was revealed, while the scatter of individual values

Figure 1 consists of two panels, (a) and (b), both showing the relationship between black hole mass and accretion rate on a log-log scale.

Panel (a) plots $M_{\text{BH}}(\text{H}\beta)/M_{\odot}$ on the y-axis (ranging from 10^5 to 10^{10}) against $M_{\text{BH}}(\text{Rev})/M_{\odot}$ on the x-axis (ranging from 10^5 to 10^{10}). Data points are shown for various sources: 20, 26, 32, and 64. Two solid lines represent different accretion efficiencies: the upper line is for $\eta = 0.1$ and the lower line is for $\eta = 0.01$. A dashed line represents the 100% accretion efficiency case ($\eta = 1$).

Panel (b) plots $M_{\text{BH}}(\text{H}\beta)/M_{\odot}$ on the y-axis (ranging from 10^5 to 10^{10}) against $M_{\text{BH}}(\text{dyn})/M_{\odot}$ on the x-axis (ranging from 10^5 to 10^{10}). Data points are shown for sources 26 and 32. A dashed line represents the 100% accretion efficiency case ($\eta = 1$).

As regards the determination of the SMBH mass from the bulge luminosity, as can be seen from Fig. 2, these estimates turn out to be systematically higher than those obtained by other methods for $M_{\text{BH}} \lesssim 10^8 M_{\odot}$ (the number of objects for comparison is too small for the corresponding conclusion to be formulated with regard to higher masses). Our regression analysis revealed no statistically significant correlation of M_{bulge} with $M_{\text{H}\beta}$ and M_{dyn} . A weakly significant correlation was found between M_{rev} and M_{bulge} , with the dependence found being in agreement with a linear one ($\beta = 1.2 \pm 0.3$). However, only one object, NGC 4395, makes a major contribution

to this correlation. It is often called a "dwarf Seyfert galaxy" (see, e.g., Peterson et al. 2005) because of an atypically low SMBH mass ($M_{\text{BH}} < 10^6 M_{\odot}$) and a low luminosity (its luminosity is much lower than that of the remaining objects in our sample, see Table 1). If we exclude NGC 4395 from consideration, then the correlation of M_{rev} with M_{bulge} (based on six objects) ceases to be statistically significant.

The main conclusion that can be drawn from this study is that the masses M_{BH} estimated from the infrared bulge luminosity are in poor agreement and, on average, are overestimated relative to the more reliable estimates of the SMBH masses in Seyfert galaxies. The differences of the correlation between the SMBH mass and the bulge luminosity for AGNs and normal galaxies have already been pointed out in several previous papers (Nelson et al. 2004; Bentz et al. 2009).

THE ACCRETION RATE

Given the SMBH mass estimate, we can calculate the Eddington limit,

$$L_{\text{Edd}} = 1.3 \times 10^{46} \frac{M_{\text{BH}}}{10^8 M_{\odot}}, \quad (14)$$

and compare it with the bolometric AGN luminosity. In our recent paper (Sazonov et al. 2012), based on the set of Spitzer infrared observations and INTEGRAL hard X-ray observations for the same sample of objects that is investigated here, we showed that the hard X-ray luminosity is a good indicator of the bolometric AGN luminosity, more specifically,

$$\frac{L_{\text{bol}}}{L_{17-60 \text{ keV}}} \sim 9. \quad (15)$$

Table 5 gives the values of L_{Edd} , L_{bol} and $L_{\text{bol}}/L_{\text{Edd}}$ obtained for our objects from these formulas using two alternative types of SMBH mass estimation: (1) M_{bulge} (from the correlation with the infrared luminosity of the bulge/elliptical galaxy); (2) the best estimate — if there is a dynamical mass estimate (M_{dyn}) for an object, then we use it; otherwise (in order of preference), the estimate by reverberation mapping (M_{rev}), from the parameters of the broad H_{β} line ($M_{H\beta}$), and from the correlation with the bulge luminosity (M_{bulge}) is used.

Formula (15) cannot be used for the Compton-thick Seyfert galaxy NGC 1068. Therefore, we estimated its bolometric luminosity from the infrared luminosity ($\lg L_{15 \mu\text{m}} = 43.87$) of the dusty torus (Mason et al. 2006) based on the relation

$$\frac{L_{\text{bol}}}{L_{15 \mu\text{m}}} \sim 5 \quad (16)$$

derived by Sazonov et al. 2012 from Spitzer observations of Seyfert galaxies from the INTEGRAL survey.

The ratio $L_{\text{bol}}/L_{\text{Edd}}$ may be considered as an indicator of the SMBH accretion regime. Figure 4 presents the values of $L_{\text{bol}}/L_{\text{Edd}}$ calculated both from the M_{bulge} estimates (a) and from the best SMBH mass estimates (b). For most of the objects, $0.01 < L_{\text{bol}}/L_{\text{Edd}} < 1$. This suggests that the gas is most likely accreted onto the SMBH in a radiatively efficient regime via a geometrically thin, optically thick disk (Shakura & Sunyaev 1973).

However, the bolometric luminosity for AGN 1H 0323+342, a narrow line Seyfert 1 (NLS1) galaxy, exceeds the Eddington one. For two more NLS1 objects, MRK 110 and 1H 1934-063, $L_{\text{bol}}/L_{\text{Edd}}$ turns out to be also high if the best SMBH mass estimate, $M_{H\beta}$, is used. In addition, M_{bulge} for 1H 1934-063 exceeds $M_{H\beta}$ by two orders of magnitude. For the remaining two NLS1 objects, IGR J14552-5133 and IGR J16185-5958, $L_{\text{bol}}/L_{\text{Edd}} = 0.03$ and 0.14 , respectively, but these estimates cannot be considered reliable, because they were obtained from M_{bulge} . On the whole, these results confirm that the most rapid SMBH growth occurs at the present epoch in narrow-line Seyfert 1 galaxies (Mathur 2000) and suggest that this growth is far from completion.

For several objects, $L_{\text{bol}}/L_{\text{Edd}} < 0.01$ (Fig. 4). This may imply that the gas is accreted onto the SMBH at a low rate and/or with a low electromagnetic wave emission efficiency. However, in all these cases, the values of $L_{\text{bol}}/L_{\text{Edd}}$ were obtained from the M_{bulge} estimates and, therefore, may be grossly underestimated.

CONCLUSIONS

Our study based on a representative sample of nearby AGNs has shown that the estimate of the SMBH masses in Seyfert galaxies from the infrared luminosity (and, consequently, from the mass) of the stellar bulge cannot be considered reliable and, on average, leads to overestimated values of M_{BH} (for $\lesssim 10^8 M_{\odot}$). This may indicate that the black hole growth in an appreciable fraction of Seyfert galaxies is still far from completion; at least we can say about this with confidence in regard to NLS1 Seyfert galaxies. However, since here we used a rather small sample of AGNs and since our estimates have considerable uncertainties (in particular, we used rather rough estimates of the bulge fraction in the galaxy's total luminosity), this conclusion cannot be deemed the final one. In addition, it is not yet clear how it is reconciled with the conclusion reached by several authors (see the Introduction) that AGNs obey the standard $M_{\text{BH}}-\sigma_*$ correlation. The ratio of the bolometric luminosity to the critical Eddington one ranges from 1 to 100% for the overwhelming majority of objects. This suggests that the gas is accreted onto the SMBHs in Seyfert galaxies at a high rate and

Table 5. Summary table of various SMBH mass estimates

Object	N ^a	$\lg M_{\text{dyn}}$ (M_{\odot})	$\lg M_{\text{rev}}$ (M_{\odot})	$\lg M_{\text{H}\beta}$ (M_{\odot})	$\lg M_{\text{bulge}}$ (M_{\odot})	$L_{\text{Edd,bulge}}$ (erg/s)	L_{bol} (erg/s)	$L_{\text{bol}}/$ $L_{\text{Edd,bulge}}$	$L_{\text{Edd,best}}$ (erg/s)	$L_{\text{bol}}/$ $L_{\text{Edd,best}}$
MRK348	1				< 7.71	< 45.81	44.51	> 0.051	< 45.81	> 0.051
MCG-01-05-047	2				7.58	45.68	43.97	0.020	45.68	0.020
NGC788	3				7.92	46.02	44.23	0.016	46.02	0.016
LEDA138501	4			8.53 ^{8.61} _{8.45}			45.29		46.63	0.046
MRK1040	5			7.77 ^{7.91} _{7.63}	7.75	45.85	44.42	0.038	45.87	0.036
IGRJ02343+3229	6				8.13	46.23	44.29	0.012	46.23	0.012
NGC1068	7	6.94 ^{6.95} _{6.92}			7.88	45.98	44.57	0.039	45.04	0.339
NGC1142	8				8.48	46.58	44.88	0.020	46.58	0.020
1H0323+342	9			7.08 ^{7.18} _{6.98}	< 8.17	< 46.27	45.32	> 0.114	45.18	1.398
NGC1365	10				7.97	46.07	43.06	0.001	46.07	0.001
3C111	11			9.08 ^{9.17} _{8.99}	< 8.97	< 47.07	45.57	> 0.032	47.18	0.025
ESO033-G002	12				7.82	45.92	44.09	0.015	45.92	0.015
IRAS05078+1626	13			7.65 ^{7.82} _{7.48}	\lesssim 7.88	\lesssim 45.98	44.56	\gtrsim 0.039	45.75	0.065
ESO005-G004	14				7.50	45.60	43.13	0.003	45.60	0.003
MRK3	15				7.96	46.06	44.38	0.021	46.06	0.021
MRK6	16				8.01	46.11	44.40	0.020	46.11	0.020
IGRJ07563-4137	17				8.02	46.12	44.03	0.008	46.12	0.008
ESO209-G012	18				8.49	46.59	44.74	0.014	46.59	0.014
IRAS09149-6206	19				\leq 9.59	\leq 47.69	45.14	\leq 0.003	\leq 47.69	\leq 0.003
MRK110	20		7.40 ^{7.49} _{7.28} (1)	7.29 ^{7.39} _{7.19}	< 7.77	< 45.87	45.16	> 0.197	45.50	0.463
IGRJ09446-2636	21				\lesssim 8.62	\lesssim 46.72	46.26	\gtrsim 0.351	46.72	0.351
NGC2992	22				7.62	45.72	43.71	0.010	45.72	0.010
MCG-5-23-16	23				7.28	45.38	44.13	0.057	45.38	0.057
NGC3081	24				7.55	45.65	43.72	0.012	45.65	0.012
ESO263-G013	25				7.98	46.08	44.67	0.039	46.08	0.039
NGC3227	26	7.18 ^{7.30} _{6.85}	7.59(2)	7.05 ^{7.25} _{6.85}	7.67	45.77	43.62	0.007	45.28	0.022
NGC3281	27				8.07	46.17	43.93	0.006	46.17	0.006
IGRJ10386-4947	28				\lesssim 8.27	\lesssim 46.37	45.04	\gtrsim 0.047	\lesssim 46.37	\gtrsim 0.047
IGRJ10404-4625	29				7.88	45.98	44.37	0.025	45.98	0.025
NGC3783	30		7.47 ^{7.54} _{7.38} (1)		7.71	45.81	44.29	0.031	45.57	0.053
IGRJ12026-5349	31				8.20	46.30	44.57	0.019	46.30	0.019
NGC4151	32	7.65 ^{7.7} _{7.6}	7.12 ^{7.25} _{6.94} (1)	7.67 ^{7.77} _{7.57}	7.61	45.71	44.32	0.041	45.75	0.038
MRK50	33			7.30 ^{7.41} _{7.19}	< 7.36	< 45.46	44.14	> 0.048	45.40	0.056
NGC4388	34				7.20	45.30	43.74	0.028	45.30	0.028
NGC4395	35		5.56 ^{5.67} _{5.40} (3)		5.01	43.11	41.55	0.028	43.66	0.008
NGC4507	36				7.81	45.91	44.46	0.036	45.91	0.036
NGC4593	37		6.99 ^{7.08} _{6.89} (4)	7.10 ^{7.22} _{6.98}	7.98	46.08	43.99	0.008	45.09	0.080
NGC4945	38	6.15 ^{6.32} _{5.95}			6.96	45.06	42.49	0.003	44.25	0.018
ESO323-G077	39				8.16	46.26	44.08	0.007	46.26	0.007
IGRJ13091+1137	40				7.91	46.01	44.63	0.042	46.01	0.042
IGRJ13149+4422	41				7.95	46.05	44.76	0.052	46.05	0.052
CENA	42				8.24	46.34	42.89	0.0004	46.34	0.0004
MCG-6-30-15	43				7.26	45.36	43.61	0.018	45.36	0.018
MRK268	44				7.95	46.05	44.74	0.050	46.05	0.050
IC4329A	45		< 7.40(1)		7.98	46.08	44.90	0.067	< 45.50	> 0.254
NGC5506	46				7.68	45.78	44.07	0.020	45.78	0.020
IGRJ14552-5133	47				7.23	45.33	43.84	0.033	45.33	0.033
IGRJ14561-3738	48				8.25	46.35	44.22	0.008	46.35	0.008
IC4518A	49				\lesssim 7.71	\lesssim 45.81	44.06	\gtrsim 0.018	\lesssim 45.81	\gtrsim 0.018
WKK6092	50				7.54	45.64	43.89	0.018	45.64	0.018
IGRJ16185-5928	51				7.39	45.49	44.62	0.137	45.49	0.137
ESO137-G34	52				8.02	46.12	43.43	0.002	46.12	0.002
IGRJ16482-3036	53				\lesssim 7.89	\lesssim 45.99	44.70	\gtrsim 0.052	\lesssim 45.99	\gtrsim 0.052
NGC6221	54				7.41	45.51	42.89	0.002	45.51	0.002
IGRJ16558-5203	55				\lesssim 9.07	\lesssim 47.17	45.24	\gtrsim 0.012	\lesssim 47.17	\gtrsim 0.012
NGC6300	56				7.59	45.69	43.02	0.002	45.69	0.002
IGRJ17418-1212	57			7.96 ^{8.38} _{7.54}	\lesssim 8.64	\lesssim 46.74	44.85	\gtrsim 0.013	46.06	0.062
3C390.3	58		8.46 ^{8.55} _{8.35} (1)	9.61 ^{9.79} _{9.43}	\lesssim 8.82	\lesssim 46.92	45.60	\gtrsim 0.048	46.56	0.111
IGRJ18559+1535	59				\lesssim 8.35	\lesssim 46.45	45.53	\gtrsim 0.122	\lesssim 46.45	\gtrsim 0.122
1H1934-063	60			6.24 ^{6.37} _{6.11}	8.13	46.23	43.58	0.002	44.34	0.176
NGC6814	61			6.91 ^{7.04} _{6.78}	7.53	45.63	43.42	0.006	45.01	0.026
CYGA	62	9.43 ^{9.53} _{9.28}			< 9.33	< 47.43	45.57	> 0.014	47.53	0.011
IGRJ20286+2544	63				7.12	45.22	44.11	0.079	45.22	0.079
MRK509	64		8.16 ^{8.20} _{8.12} (1)	8.22 ^{8.32} _{8.12}	8.15	46.25	45.11	0.073	46.26	0.072
NGC7172	65				7.81	45.91	43.87	0.009	45.91	0.009
MR2251-178	66			8.71 ^{8.82} _{8.6}	< 9.08	< 47.18	45.60	> 0.027	46.81	0.062
NGC7469	67		7.09 ^{7.14} _{7.04} (1)	7.56 ^{7.69} _{7.43}	8.18	46.28	44.38	0.013	45.19	0.157
MRK926	68			8.73 ^{8.83} _{8.63}	< 8.44	< 46.54	45.20	> 0.046	46.83	0.024

Note. M_{dyn} is the dynamical mass estimate (Gültekin et al. 2009); M_{rev} is the reverberation-based mass estimate from: (1) Peterson et al. (2004), (2) Onken & Peterson (2002), (3) Peterson et al. (2005), (4) Denney et al. (2006); $M_{\text{H}\beta}$ is the mass estimate from the parameters of the broad $\text{H}\beta$ line (RTT-150); M_{bulge} is the mass estimate from the bulge luminosity (2MASS); L_{bol} is the bolometric luminosity; $L_{\text{Edd,bulge}}$ is the Eddington luminosity calculated from M_{bulge} ; $L_{\text{Edd,best}}$ is the Eddington luminosity calculated from the best mass estimate.

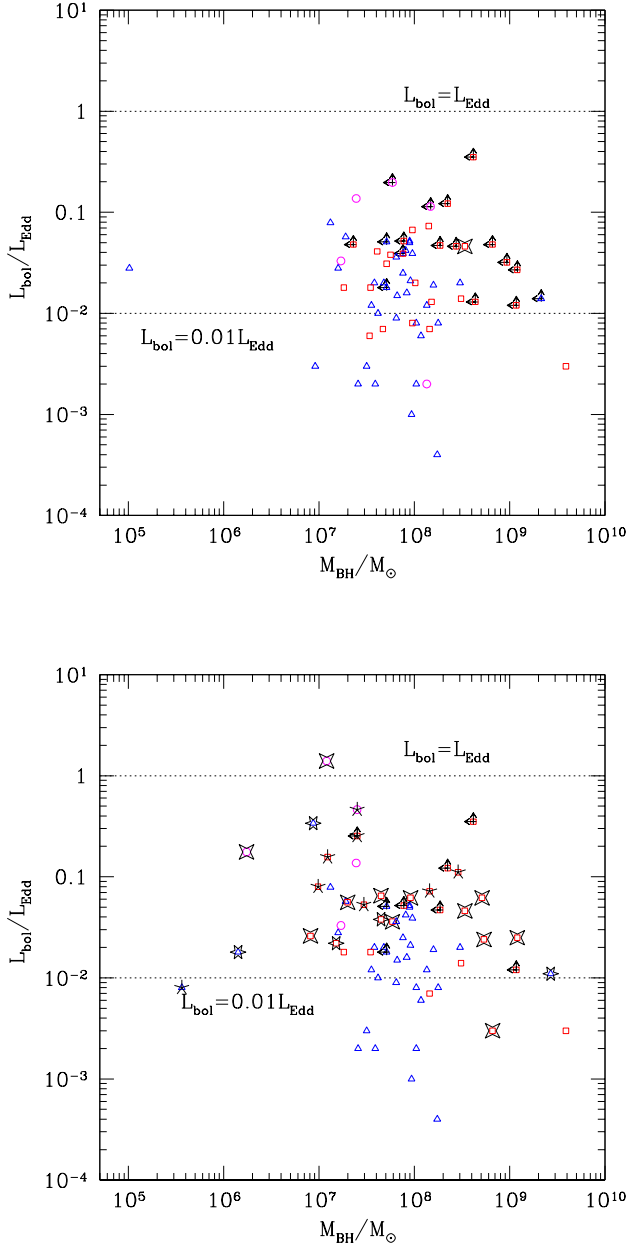


Fig. 4. *Top*: Bolometric-to-Eddington AGN luminosity ratio versus SMBH mass. M_{BH} was estimated from the infrared bulge luminosity, except for LEDA 138501 (marked by the four-point star) for which the estimate from the parameters of the broad H_{β} line is presented. The Seyfert 1, 2, and narrow-line Seyfert 1 (NLS1) galaxies are marked by the squares, triangles, and circles, respectively. The measurement uncertainties are not shown. *Bottom*: The same, only based on the best mass estimates: M_{dyn} (six-point stars), M_{rev} (five-point stars), $M_{\text{H}\beta}$ (four-point stars), M_{bulge} (remaining points).

in a radiatively efficient regime. This conclusion is consistent with the results of previous studies (see, e.g., Middleton et al. (2008), de Rosa et al. (2012)).

ACKNOWLEDGMENTS

We wish to thank the referee for a number of useful remarks. We used data from the Russian–Turkish 1.5-m telescope, the 2MASS survey (University of Massachusetts, IPAC), and the NASA/IPAC/NED (Jet Propulsion Laboratory, California Institute of Technology), VizieR (CDS, Strasbourg), and HyperLeda (Observatoire de Lyon) databases. This study was supported by the Russian Foundation for Basic Research (project nos. 09-02-00867-a, 10-02- 01442-a, 11-02-12285-ofi-m-2011, 11-02-12271- ofi-m), Programs P-21 and OFN-16 of the Russian Academy of Sciences, and the Program for Support of Leading Scientific Schools of the Russian Federation (NSh-5069.2010.2).

REFERENCES

1. M.C. Bentz, B.M. Peterson, R.W. Pogge, et al., *Astrophys. J.* **694**, L166 (2009).
2. J.A. Cardelli, G.C. Clayton, & J.S. Mathis, *Astrophys. J.* **345**, 245 (1989).
3. K.D. Denney, M.C. Bentz, B. Peterson, et al., *Astrophys. J.* **653**, 152 (2006).
4. A. de Rosa, F. Panessa, L. Bassani, et al., *Mon. Not. R. Astron. Soc.* **420**, 2087 (2012).
5. E.A. Dibai, *Письма в Астрон. журн.* **3**, 3 (1977).
6. X. Dong, T. Wang, J. Wang, et al., *Mon. Not. R. Astron. Soc.* **383**, 581 (2008).
7. M. Elvis, B.J. Wilkes, J.C. McDowell, et al., *Astrophys. J. Suppl. Ser.* **95**, 1 (1994).
8. L. Ferrarese, & D. Merritt, *Astrophys. J.* **539**, L9 (2000).
9. A.W. Graham, *Mon. Not. R. Astron. Soc.* **379**, 711 (2007).
10. A.W. Graham, C.C. Worley, *Mon. Not. R. Astron. Soc.* **388**, 1708 (2008).
11. A.W. Graham, C.A. Onken, E. Athanassoula & F. Combes, *Mon. Not. R. Astron. Soc.* **412**, 2211 (2011).
12. D. Grupe, S. Mathur, *Astrophys. J.* **606**, L41 (2004).
13. K. Gültekin, D. Richstone, K. Gebhardt, et al., *Astrophys. J.* **698**, 198 (2009).
14. T.H. Jarrett, T. Chester, R. Cutri, et al., *Astron. J.* **119**, 2498 (2000).
15. T.H. Jarrett, T. Chester, R. Cutri, et al., *Astron. J.* **125**, 525 (2003).
16. S. Kaspi, P.S. Smith, H. Netzer, et al., *Astrophys. J.* **533**, 631 (2000).
17. S. Kaspi, D. Maoz, H. Netzer, et al., *Astrophys. J.* **629**, 61 (2005).
18. R. Krivonos, M. Revnivtsev, A. Lutovinov, et al., *Astron. Astrophys.* **475**, 775 (2007).

19. E. Laurikainen, H. Salo, R. Buta, et al., *Mon. Not. R. Astron. Soc.* **381**, 401 (2007).
20. E. Laurikainen, H. Salo, R. Buta, et al., *Mon. Not. R. Astron. Soc.* **405**, 1089 (2010).
21. A. Marconi, & L.K. Hunt, *Astrophys. J.* **589**, L21 (2003).
22. R.E. Mason, T.R. Geballe, C. Packham, et al., *Astrophys. J.* **640**, 612 (2006).
23. S. Mathur, *Mon. Not. R. Astron. Soc.* **314**, L17 (2000).
24. S. Mathur, J. Kuraszewicz, B. Czerny, *NewA* **6**, 321 (2001).
25. M. Middleton, C. Done, N. Schurch, *Mon. Not. R. Astron. Soc.* **383**, 1501 (2008).
26. C. H. Nelson, R.F. Green, G. Bower, et al., *Astrophys. J.* **615**, 652 (2004).
27. H.U. Norgaard-Nielsen, L. Hansen, H.E. Jorgensen, et al., *Astron. Astrophys.* **169**, 49 (1986).
28. C.A. Onken, L. Ferrarese, D. Merritt, et al., *Astrophys. J.* **615**, 645 (2004).
29. C.A. Onken, B.M. Peterson, *Astrophys. J.* **572**, 746 (2002).
30. B.M. Peterson, L. Ferrarese, K. Gilbert et al., *Astrophys. J.* **613**, 682 (2004).
31. B.M. Peterson, M.C. Bentz, L. Desroches, et al., *Astrophys. J.* **632**, 799 (2005).
32. A. Petrosian, B. McLean, R.J. Allen, et al., *Astrophys. J. Suppl. Ser.* **170**, 33 (2007).
33. W.H. Press, S.A. Teukolsky, W.T. Vetterling, et al., *Numerical Recipes 2d ed.*; Cambridge: Cambridge Univ. Press (1992)
34. G.T. Richards, M. Lacy, L.J. Storie-Lombardi, et al., *Astrophys. J. Suppl. Ser.* **166**, 470 (2006).
35. S.Y. Sazonov, J.P. Ostriker, & R.A. Sunyaev, *Mon. Not. R. Astron. Soc.* **347**, 144 (2004).
36. S. Sazonov, M. Revnivtsev, R. Krivonos et al., *Astron. Astrophys.* **462**, 57 (2007).
37. S. Sazonov, R. Krivonos, M. Revnivtsev et al., *Astron. Astrophys.* **482**, 517 (2008).
38. S. Sazonov, S. Willner, M. Churazov, et al., *Astrophys. J.* **757**, 181 (2012). (in press)
39. D.J. Schlegel, D.P. Finkbeiner, M. Davis, et al., *Astrophys. J.* **500**, 525 (1998).
40. N.I. Shakura, & R.A. Sunyaev, *Astron. Astrophys.* **24**, 337 (1973).
41. Z. Shang, M.S. Brotherton, B.J. Wills, et al., *Astrophys. J. Suppl. Ser.* **196**, 2 (2011).
42. M.F. Skrutskie, R.M. Cutri, R. Stiening, et al., *Astron. J.* **131**, 1163 (2006).
43. S. Tremaine, K. Gebhardt, R. Bender, et al., *Astrophys. J.* **574**, 740 (2002).
44. Талли (R.B. Tully), 1988, *Nearby Galaxies Catalogue*, Cambridge University Press
45. R.B. Tully, L. Rizzi, E.J. Shaya, et al., *Astron. J.* **138**, 323 (2009).
46. P. Ubertini, F. Lebrun, G. Di Cocco, et al., *Astron. Astrophys.* **411**, L131 (2003).
47. M. Vestergaard & B.M. Peterson, *Astrophys. J.* **641**, 689 (2006).
48. A. Wandel, *Astrophys. J.* **519**, L39 (1999).
49. A. Wandel, *Astrophys. J.* **565**, 762 (2002).
50. A. Wandel, B.M. Peterson & M.A. Malkan, *Astrophys. J.* **526**, 579 (1999).
51. C. Winkler, T.J.-L. Courvoisier, G. Di Cocco, et al., *Astron. Astrophys.* **411**, L1 (2003).
52. J.-H. Woo, T. Treu, A.J. Barth, et al., *Astrophys. J.* **716**, 269 (2010).
53. H. Zhou, T. Wang, W. Yuan, et al., *Astrophys. J.* **658**, L13 (2007).

Translated by V. Astakhov